

# System and Design Technology Co-optimization of SOT-MRAM for High-Performance AI Accelerator Memory System

Kaniz Mishty and Mehdi Sadi, *Member, IEEE*,

**Abstract**—SoCs are now designed with their own AI accelerator segment to accommodate the ever-increasing demand of Deep Learning (DL) applications. With powerful MAC engines for matrix multiplications, these accelerators show high computing performance. However, because of limited memory resources (i.e., bandwidth and capacity), they fail to achieve optimum system performance during large batch training and inference. In this work, we propose a memory system with high on-chip capacity and bandwidth to shift the gear of AI accelerators from memory-bound to achieving system-level peak performance. We develop the memory system with DTCO-enabled customized SOT-MRAM as large on-chip memory through STCO and detailed characterization of the DL workloads. Our workload-aware memory system achieves  $8\times$  energy and  $9\times$  latency improvement on Computer Vision (CV) benchmarks in training and  $8\times$  energy and  $4.5\times$  latency improvement on Natural Language Processing (NLP) benchmarks in training while consuming only around 50% of SRAM area at iso-capacity.

**Index Terms**—DTCO, STCO, AI/Deep Learning Accelerator, SOT-MRAM.

## 1 INTRODUCTION

THE proliferation of Artificial Intelligence (AI) and Deep Learning (DL) has precipitated the computing hardware community to continually design innovative AI/DL accelerators with large data processing capabilities. Research shows that the AI/DL model accuracy improves as training data set size grows [1]. With increasing data set, model size also grows. Consequently, memory demand in AI/DL accelerators will also grow asymptotically linearly with model and data size [1] [2]. As a result, the bottleneck for state-of-the-art AI/DL models in the accelerator hardware is now memory rather than data and compute availability, and we expect this trend to worsen in the future [2] [3] [4].

The lack of efficient and high-performance data flow between the computing and memory element (i.e., the memory wall or memory bottleneck) masks the improvement coming from the efficient compute system [5]. One promising solution to the memory bottleneck of AI-specific workload is to increase the on-chip memory capacity [6]. For both training and inference, the on-chip memory capacity in the accelerator needs to be increased to ensure that the intermediate activations, as well as the weights of the current layer, can be loaded. Moreover, significantly more memory is required during training to store the gradients and optimizer states. Inadequate on-chip memory capacity will cause frequent DRAM accesses which will exacerbate energy costs, as well as stall the compute cores of AI/DL accelerator until the data is fetched. Because of this large capacity demand,

an SRAM-based on-chip memory system can be detrimental due to leakage energy and area inefficiency.

The promising features, such as high density, near-zero leakage power, immunity against radiation-induced soft errors, and CMOS compatibility of emerging Spin-based non-volatile (NVM) magnetic memory (i.e., MRAM) technologies, attracted researchers from academia and industry [7]. Spin Transfer Torque (STT) MRAM, has already shifted its gear from the R&D phase to commercialization as the NAND-based embedded flash replacement [8] [9]. However, MRAM in its regular form cannot be used in AI accelerators due to its slow write speed and high write energy [9] [10].

STT-MRAM, a two-terminal magnetic memory with Magnetic Tunnel Junction (MTJ) as the storing element, flows a bidirectional spin-polarized current through the MTJ for read-write operation [11]. The major challenges of STT-MRAM, such as poor write performance, reliability issues, e.g., Read Disturbance (RD), retention failure, [9] [12], stem from two main reasons. First, the high write current flowing through the MTJ accounts for almost  $10\times$  energy consumption as SRAM. Large write delay ( $> \text{ns}$  range) resulting from spin injection symmetry in switching the magnetic orientation of free layer belittles STT-MRAM's feasibility as an on-chip cache [13]. The stress on the dielectric oxide of the MTJ due to the large write current accelerates the time-dependent wear out of the cell [14]. Second, its shared read-write path makes it vulnerable to RD.

Spin-Orbit Torque (SOT) MRAM, considered the next generation of STT-MRAM, offers high performance without compromising reliability issues such as RD. SOT-MRAM is a four-terminal memory cell that uses MTJ as the storing element [15]. By splitting the read-write path and using a different switching scheme, SOT-MRAM resolves all the challenges of STT-MRAM while retaining its every benefit [9] [12] [13] [14] [16]. Isolate read and write path allows the

• The authors are with the Department of Electrical and Computer Engineering, Auburn University, Auburn, AL 36849 USA  
E-mail: kzm0114@auburn.edu; mehdi.sadi@auburn.edu

This work was supported in part by the National Science Foundation under Grant Number CRII-2153394.

Manuscript received November XX, 2022; revised month XX, 2023.

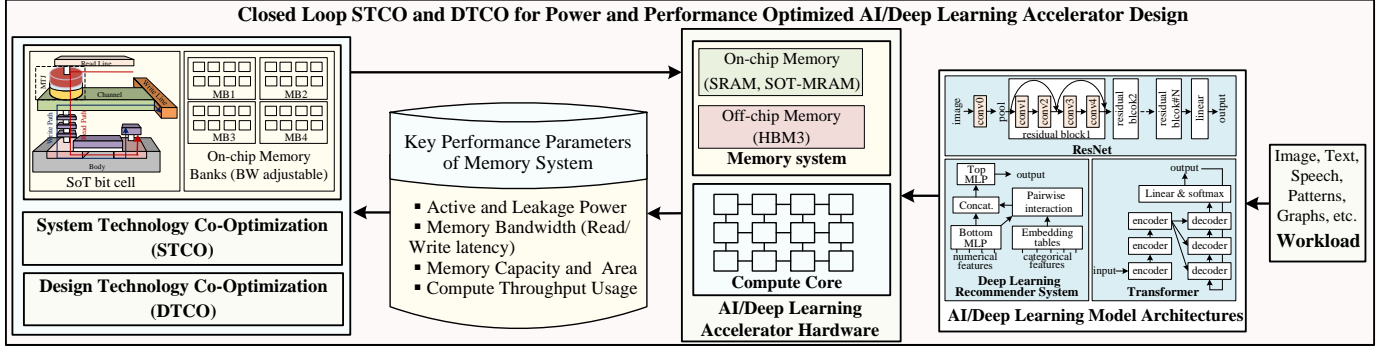


Fig. 1. Workflow of closed-loop analysis for system and device level optimization for AI/Deep Learning Accelerator Design

designer to optimize the read and write path independently, decreasing the write current and increasing the read-write operating margin, thus solving the RD-induced reliability issues. Though lacking mass-scale production from foundries due to early-stage manufacturing challenges, [9] [10] [12] [13] [16] [17] have demonstrated the successful fabrication of SOT-MRAM with attractive specifications. Its attractive features, such as high density, reliability and endurance, zero leakage, read-write latency comparable to SRAM, and research effort to enable mass production make it one of the best candidates for AI accelerator memory system where large on-chip memory is a must for training and inference.

The performance of an AI accelerator depends on both the compute and memory throughput of the device. While most accelerators have enough compute throughput, their performance is limited by memory throughput operating in the *memory bound* region. To address the *memory bound* problem of the AI hardware, in this paper, we perform a closed-loop STCO on AI workloads and DTCO on SOT-MRAM to present a hybrid memory system. To our knowledge, this is the first work that analyzes and evaluates the performance of SOT-MRAM as the on-chip memory of AI accelerators targeting both inference and training. The STCO-DTCO methodology is shown in Fig. 1, and the key contributions of the paper are highlighted as follows.

- We present a power and performance-optimized hybrid memory system for Deep Learning (DL) accelerators through a workload-aware STCO and DTCO. Comprised of off-chip HBM3 DRAM, on-chip SRAMs, and DTCO-enabled SOT-MRAM, the hybrid memory system can support the training and inference of DL workloads. We perform a closed-loop STCO and DTCO by taking into account the (i) System performance attributes (e.g., throughput and energy cost); (ii) Architectural and micro-architectural attributes (e.g., compute resources utilization, memory bandwidth) (iii) Workload attributes at both training and inference (e.g., runtime action counts, dataflow and data reuse) to reach the Pareto optimal solution.
- Using the Deep Learning models' execution profiles, DTCO enables device and circuit level customization of read/write bandwidth, retention time, and capacity of SOT-MRAM memory banks to meet the bandwidth and capacity demands of DL workloads. Moreover, to achieve dynamic runtime optimization of the power

and performance of the accelerator hardware for diverse workloads, memory banks are individually optimized with various bandwidths and capacities.

- Finally, using various DNN benchmarks, we provide a comparative analysis of the existing SRAM-based memory system and the proposed DTCO-STCO optimized hybrid memory system for AI accelerators.

The rest of the article is organized as follows. Section 2 discusses the background. In Section 3, we present the analytical model for DNN workload profiling, followed by the DTCO of SOT-MRAM in Section 4. Sections 5 and 6 present the results & analysis, and related works, respectively, following the conclusion in Section 7.

## 2 BACKGROUND

### 2.1 AI/DL Applications

#### 2.1.1 Computer Vision (CV) and Pattern Recognition

CV is one of the earliest applications of DL. CV models are the stacks of convolution layers to extract the objects' features and a few FC layers at the end to classify them (Fig. 4). Image classification, object detection, object/instance segmentation, image reconstruction, and captioning are the scopes of CV models. Image captioning combines both CV and NLP tasks.

#### 2.1.2 Natural Language Processing (NLP)

Language modeling deals with processing sequential data. Recurrent Neural Networks (RNN), Long Short Term Memory (LSTM), and Gated Recurrent Unit (GRU) have been used in language modeling until the state-of-the-art Transformer [18] model is introduced. NLP models are used in machine translation, text summarization, speech recognition, syntactic and semantic parsing, question answering, dialog system etc.

### 2.2 AI/DL Accelerators

At the core of AI/DLs is the matrix-matrix/vector multiplication (GEMM) with massive parallelism. Exploiting this parallelism, SIMD and Systolic Array (SA) based architecture have been used to accelerate the computations. Different dataflows, such as row stationary, output stationary, weight stationary, have been evolved to maximize the reuse and reduce the data movement. Off-chip DRAM access being 100-200 times more energy and latency expensive than any ALU operation or on-chip access [19] plays a crucial role in

determining the overall system performance. In this work, we focus on reducing the off-chip memory access by increasing the on-chip Global Buffer (GLB) size with SOT-MRAM.

## 2.3 SOT-MRAM

### 2.3.1 Physical Structure

With MTJ [11] as storing element, the SOT-MRAM is a four terminal device: (i) *Read Wordline (RWL)*, (ii) *Write Wordline (WWL)*, (iii) *Bit Line (BL)*, and (iv) *Bit Linebar (BLB)* [15] (Fig. 2). The MTJ stack, with its free layer at the interface, is placed on top of a SOT layer (also known as the channel) to ensure SOT induced switching. The SOT layer is composed of heavy metals or topological insulators [20]. Two access transistors are used to access the separate read and write path.

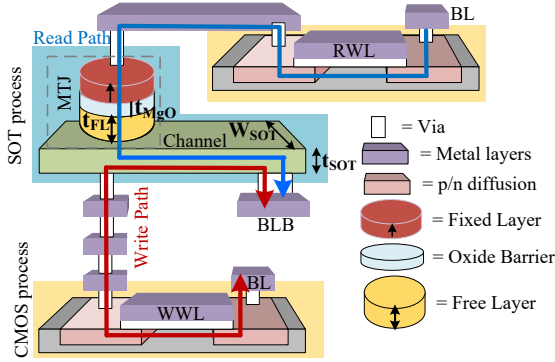


Fig. 2. Physical structure of a SOT-MRAM bit cell highlighting separate read (along blue line) and write (along red line) path

### 2.3.2 Read-Write Operation

Upon the activation of RWL, a small amount of current is passed through BL and grounded BLB. The resistive state of the MTJ is captured by sensing the voltage across it and comparing the voltage with a reference value [12]. Low resistive state ( $R_P$ ) and high resistive state ( $R_{AP}$ ) represents bit 0 and 1 respectively.

The write operation of MTJ-based MRAM involves switching the resistive status of MTJ. In SOT-MRAM, switching occurs due to Spin Orbit Torque (SOT) effect. Unlike STT-MRAM, a current is passed through the SOT layer to change the MTJ resistive state by switching the magnetic orientation of the free layer. In the write operation, a bidirectional write current flows through BL and BLB. The potential of BL and BLB changes depending on the bit value written in the cell. For example, to write 1, current flows from BL to BLB and vice versa to write 0 [12] [14].

## 3 DNN WORKLOAD PROFILING

Profiling the target workload is a prerequisite for designing an accelerator for the target workload. Assuming that we have a powerful computing system to handle the exhaustive computations of the DL workload, we focus on providing efficient data movement between the compute and memory system to ensure 100% utilization of computing resources by introducing the workload-aware hybrid memory system. We propose the hybrid memory system by analyzing the Deep Learning model workloads from Computer Vision

(CV) and Natural Language Processing (NLP) domain. We analytically model the on-chip bandwidth requirement and memory access patterns of different parts of the workload during inference and training, *Memory and Compute Model*, to develop the memory system.

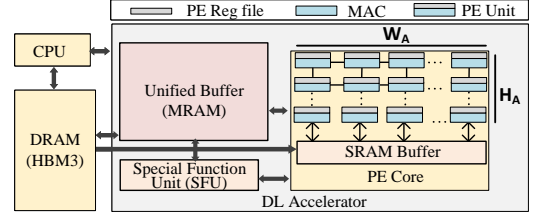


Fig. 3. Block diagram of Accelerator architecture

### 3.1 Memory Bandwidth Expression

We express the required bandwidth (BW) as a function of compute resources and workload.  $BW$  (bytes/sec) is defined as the rate at which data needs to be transferred to/from memory by a processor to fully utilize the computation resources of the processor. Mathematically,

$$BW = \frac{F_p}{OI} \quad (1)$$

Where  $F_p$  = Theoretical peak performance of accelerator (ops/sec) = number of operations the accelerator performs per sec. The  $F_p$  of a  $H_A \times W_A$  Processing Element (PE) array (Fig. 3):

$$F_p = H_A * W_A * F_{acc} \quad (2)$$

$F_{acc}$  = Operating frequency of the accelerator.  $OI$  = Operational Intensity of Workload (ops/byte) = number of operations performed by the accelerator per byte. It is a workload-dependent parameter and a measure of parallelism of the workload. In the subsequent subsections, we will formulate the  $OI$  of Conv. and Fully-Connected (FC) layer to find their BW, respectively. Note that the read and write bandwidth will not be the same for these workloads.

#### 3.1.1 Read Bandwidth ( $BW_{RD}$ ) of Conv. layer

To formulate an expression for  $OI$  of convolution workload: First, we determine the total number of MAC operations,  $T_{MAC}$ , performed by a  $H_A \times W_A$  PE array per clock cycle

$$T_{MAC} = H_A * W_A \quad (3)$$

Second, we figure out how many bytes should be read from memory to utilize all PEs of the accelerator in one clock cycle. In a row stationary dataflow [19], it takes  $(k_h * k_w + of_h * of_w) * d_w$  bytes of data ( $d_w$  = data type in bytes, i.e., FP32, BF16 etc.) and  $\#(of_h * of_w * k_h * k_w)$  PEs to generate the partial ofmaps corresponding to one input channel. Depending on the size of the PE array, in each iteration (one complete use of accelerator), multiple input channels can be fit. The input channels (i.e., no. of partial ofmaps) computed by the PE array in each iteration:

$$N_{ich\_per\_stp} = \frac{H_A * W_A}{of_h * of_w * k_h * k_w} \quad (4)$$

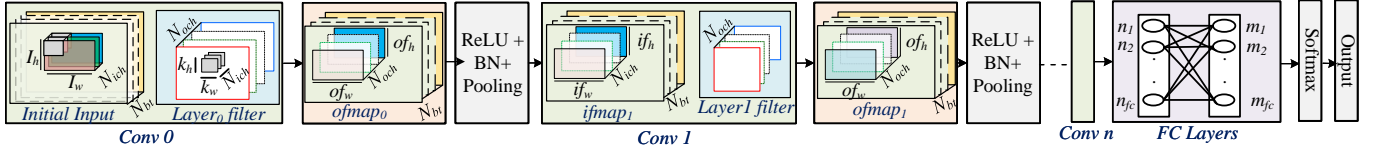


Fig. 4. CV models workflow breakdown

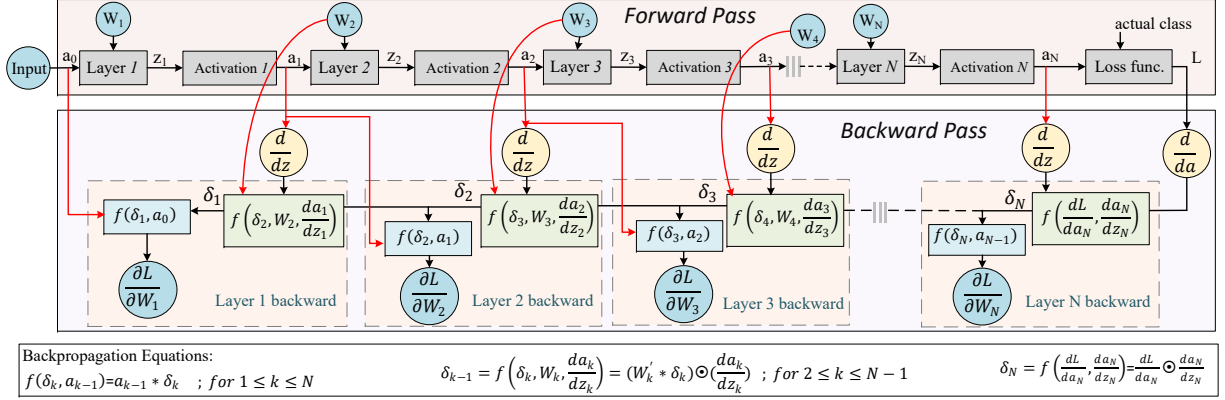


Fig. 5. Computational graph of DNN training

Total bytes read from memory to utilize all PEs:

$$T_{byte} = \frac{H_A * W_A}{k_h * k_w * of_h * of_w * (k_h * k_w + if_h * if_w) * d_w} * \quad (5)$$

We divide the total number of MAC operations,  $T_{MAC}$ , by the total bytes accessed,  $T_{byte}$ , to find  $OI$ :

$$OI = \frac{k_h * k_w * of_h * of_w}{d_w * (k_h * k_w + if_h * if_w)} \quad (6)$$

Substituting the expression of  $OI$  in equation (1) gives  $BW_{RD}$  as a function of array size and workload:

$$BW_{RD} = \frac{(k_h * k_w + if_h * if_w) * d_w}{k_w * k_h * of_h * of_w} * \frac{H_A * W_A * F_{acc}}{H_A * W_A * F_{acc}} \quad (7)$$

For the symbol meanings please see Fig. 4.

### 3.1.2 Write Bandwidth ( $BW_{WR}$ ) of Conv. Layer

Partial ofmap of a single input channel requires  $\#(of_h * of_w * k_h * k_w)$  PEs. Therefore,  $H_A \times W_A$  PEs generate  $(H_A * W_A) / (of_h * of_w * k_h * k_w)$  ofmaps in each iteration. Each partial ofmap contains  $of_h * of_w$  elements. The total output bytes generated by the PE array in one iteration is, equivalently, the write bandwidth is:

$$BW_{WR} = \frac{H_A * W_A * F_{acc} * d_w}{k_h * k_w} \quad (8)$$

### 3.1.3 $BW_{RD}$ & $BW_{WR}$ of FC layer

The systolic array is a widely used architecture to perform GEMM operation [3]. Depending on the array dimension ( $H_A \times W_A$ ) and operand matrix dimension (input matrix:  $K \times M$ , weight matrix:  $M \times N$ , and output matrix:  $K \times N$ ), we formulate required Read and Write GLB bandwidth for

TABLE 1  
RD/WR bandwidth expression of FC layer for different cases

Cases		$BW_{RD}$	$BW_{WR}$
$M < H_A; N < W_A$	$K < W_A$	$\frac{M*N+K*M}{N+K}$	$\frac{K*N}{2*N+K-1}$
	$K \geq W_A$	$\frac{M*N+W_A*M}{N+W_A}$	$\frac{W_A*N}{2*N+K-1}$
$M < H_A; N \geq W_A$	$K < W_A$	$\frac{M*W_A+K*M}{N+K}$	$\frac{K*W_A}{2*W_A+K-1}$
	$K \geq W_A$	$\frac{M*W_A+W_A*M}{2*W_A}$	$\frac{W_A^2}{2*W_A+K-1}$
$M \geq H_A; N < W_A$	$K < W_A$	$\frac{H_A*N+K*H_A}{N+K}$	$\frac{K*N}{2*N+K-1}$
	$K \geq W_A$	$\frac{H_A*N+W_A*H_A}{W_A+N}$	$\frac{W_A*N}{2*N+K-1}$
$M \geq H_A; N \geq W_A$	$K < W_A$	$\frac{H_A*W_A+W_A*H_A}{W_A+K}$	$\frac{W_A*N}{2*N+K-1}$
	$K \geq W_A$	$\frac{H_A*W_A+W_A*H_A}{2*W_A}$	$\frac{W_A^2}{2*W_A+K-1}$

four different cases: (i) Weight matrix dimensions (both) are less than the systolic array dimensions ( $M < H_A, N < W_A$ ), (ii) Height of weight matrix is less than the height of systolic array, but the width of weight matrix is larger than or equal to the width of the systolic array ( $M < H_A, N \geq W_A$ ), (iii) Height of weight matrix is larger than or equal to the height of systolic array, but width of the weight matrix is less than the width of the systolic array ( $M \geq H_A, N < W_A$ ), and (iv) Both height and width of weight matrix are larger than or equal to the height and width of systolic array respectively ( $M \geq H_A, N \geq W_A$ ).

In a weight stationary dataflow, it takes  $N$  clock cycles to load the weight matrix into the systolic array. Once the weights are loaded, the input matrix is streamed from left to right and the outputs are collected downward. The input matrix's first column reaches the weight matrix's last column at  $2N$  clock cycles. The last (or  $K^{th}$ ) column of the input matrix reaches the last column of weight matrix after  $2N +$

TABLE 2  
Architecture-and-platform-agnostic Memory access and Dataflow of CV model workload during inference and training

Data Entity	Data Dimension	Memory Access		Dataflow & Reuse Status	
		Inference	Training	Inference	Training
Initial Input (I)	$I_h \times I_w \times N_{ich} \times N_{bt}$	<ul style="list-style-type: none"> <li>• <b>HBM3 DRAM</b> Read: Once*, if <math>UB \geq I</math>, else, multiple* Write: No write back</li> <li>• <b>Unified Buffer (UB)</b> Read: UB <math>\rightarrow</math> PE core: Once* UB <math>\rightarrow</math> HBM3: None Write: PE core <math>\rightarrow</math> UB: None HBM3 <math>\rightarrow</math> UB: Once*, if <math>UB \geq I</math>, else multiple*</li> </ul>	<ul style="list-style-type: none"> <li>• <b>HBM3 DRAM</b> Read: Once*, if <math>UB \geq I</math>, else multiple* Write: No write back</li> <li>• <b>Unified Buffer (UB)</b> Read: UB <math>\rightarrow</math> PE core: At least twice* (one during forward pass, one during backward pass to calculate gradient) UB <math>\rightarrow</math> HBM3: None Write: HBM3 <math>\rightarrow</math> UB: Once*, if <math>UB \geq I</math>, else multiple* PE core <math>\rightarrow</math> UB: None</li> </ul>	<ul style="list-style-type: none"> <li>• <b>Dataflow</b> HBM3 <math>\rightarrow</math> UB <math>\rightarrow</math> PE core</li> <li>• <b>Reuse in PE core</b> Multiple times for convolutional reuse and over different filters</li> </ul>	<ul style="list-style-type: none"> <li>• <b>Dataflow</b> Forward: HBM3 <math>\rightarrow</math> UB <math>\rightarrow</math> PE core Backward: UB <math>\rightarrow</math> PE core</li> <li>• <b>Reuse in PE core</b> Forward: Multiple times for convolutional reuse and over different filters Backward: Multiple times for gradient calculation of different filters</li> </ul>
Output feature map (OFMAP)	Conv. Layer: $of_h \times of_w \times N_{och} \times N_{bt}$	<ul style="list-style-type: none"> <li>• <b>HBM3 DRAM</b> Read &amp; Write: None, if <math>UB \geq OFMAP</math>, else multiple*</li> <li>• <b>Unified Buffer (UB)</b> Read: UB <math>\rightarrow</math> PE core: None UB <math>\rightarrow</math> HBM3: None, if <math>UB \geq OFMAP</math>, else multiple*</li> <li>Write: PE core <math>\rightarrow</math> UB: Once* HBM3 <math>\rightarrow</math> UB: None</li> <li>• <b>SRAM</b> Multiple* R/W for partial OFMAP storage and local reuse</li> </ul>	<ul style="list-style-type: none"> <li>• <b>HBM3 DRAM</b> Read &amp; Write: None, if <math>UB \geq OFMAP</math>, else multiple*</li> <li>• <b>Unified Buffer (UB)</b> Read: UB <math>\rightarrow</math> PE core: None UB <math>\rightarrow</math> HBM3: None, if <math>UB \geq OFMAP</math>, else multiple*</li> <li>Write: PE core <math>\rightarrow</math> UB: Once* HBM3 <math>\rightarrow</math> UB: None</li> <li>• <b>SRAM</b> Multiple* R/W for partial OFMAP storage and local reuse</li> </ul>	<ul style="list-style-type: none"> <li>• <b>Dataflow</b> PE core <math>\rightarrow</math> SRAM <math>\rightarrow</math> UB</li> <li>• <b>Reuse in PE core</b> Multiple times for partial sum generation</li> </ul>	<ul style="list-style-type: none"> <li>• <b>Dataflow</b> Forward: PE core <math>\rightarrow</math> SRAM <math>\rightarrow</math> UB Backward: Not Applicable (N/A)</li> <li>• <b>Reuse in PE core</b> Forward: Multiple times for partial sum generation Backward: Not Applicable (N/A)</li> </ul>
	FC Layer: $N_{bt} \times m_{fc}$	<ul style="list-style-type: none"> <li>Write: PE core <math>\rightarrow</math> UB: Once* HBM3 <math>\rightarrow</math> UB: None</li> </ul>	<ul style="list-style-type: none"> <li>Write: PE core <math>\rightarrow</math> UB: Once* HBM3 <math>\rightarrow</math> UB: None</li> </ul>		
Input feature map (IFMAP)	Conv. Layer: $if_h \times if_w \times N_{ich} \times N_{bt}$	<ul style="list-style-type: none"> <li>• <b>HBM3 DRAM</b> Read &amp; Write: None, if <math>UB \geq IFMAP</math>, else multiple*</li> <li>• <b>Unified Buffer (UB)</b> Read: UB <math>\rightarrow</math> PE core: Once* UB <math>\rightarrow</math> HBM3: None Write: PE core <math>\rightarrow</math> UB: None HBM3 <math>\rightarrow</math> UB: None, if <math>UB \geq IFMAP</math>, else multiple*</li> </ul>	<ul style="list-style-type: none"> <li>• <b>HBM3 DRAM</b> Read &amp; Write: None, if <math>UB \geq IFMAP</math>, else multiple*</li> <li>• <b>Unified Buffer (UB)</b> Read: UB <math>\rightarrow</math> PE core: At least twice* (one during forward pass, one during backward pass to calculate gradient) UB <math>\rightarrow</math> HBM3: None Write: PE core <math>\rightarrow</math> UB: None HBM3 <math>\rightarrow</math> UB: None, if <math>UB \geq IFMAP</math>, else multiple*</li> </ul>	<ul style="list-style-type: none"> <li>• <b>Dataflow</b> UB <math>\rightarrow</math> PE core</li> <li>• <b>Reuse in PE core</b> Multiple times for convolutional reuse and over multiple filters</li> </ul>	<ul style="list-style-type: none"> <li>• <b>Dataflow</b> Forward &amp; Backward: UB <math>\rightarrow</math> PE core</li> <li>• <b>Reuse in PE core</b> Forward: Multiple times for convolutional reuse and over multiple filters Backward: Multiple times for gradient calculation of multiple filters</li> </ul>
	FC Layer: $N_{bt} \times n_{fc}$	<ul style="list-style-type: none"> <li>Write: PE core <math>\rightarrow</math> UB: None HBM3 <math>\rightarrow</math> UB: None, if <math>UB \geq IFMAP</math>, else multiple*</li> </ul>	<ul style="list-style-type: none"> <li>Write: PE core <math>\rightarrow</math> UB: None HBM3 <math>\rightarrow</math> UB: None, if <math>UB \geq IFMAP</math>, else multiple*</li> </ul>		
Weights (W)	Conv. Layer: $k_h \times k_w \times N_{ich} \times N_{och}$	<ul style="list-style-type: none"> <li>• <b>HBM3 DRAM</b> Read: Once, if <math>H_A \times W_A \geq W</math>, else multiple* Write: No write back</li> <li>• <b>Unified Buffer (UB)</b> Read &amp; Write: None</li> </ul>	<ul style="list-style-type: none"> <li>• <b>HBM3 DRAM</b> Read: Once*, if <math>UB \geq W</math>, else multiple* Write: Once* (to write the trained weights)</li> <li>• <b>Unified Buffer (UB)</b> Read: UB <math>\rightarrow</math> PE core: At least thrice* (for forward pass, input gradient calculation, and trained filter weights) UB <math>\rightarrow</math> HBM3: Once* Write: PE core <math>\rightarrow</math> UB: At least once* HBM3 <math>\rightarrow</math> UB: Once*, if <math>UB \geq W</math>, else multiple*</li> </ul>	<ul style="list-style-type: none"> <li>• <b>Dataflow</b> HBM3 <math>\rightarrow</math> PE core / SRAM</li> <li>• <b>Reuse in PE core</b> Multiple times for convolutional reuse and for different samples of minibatch</li> </ul>	<ul style="list-style-type: none"> <li>• <b>Dataflow</b> Forward: HBM3 <math>\rightarrow</math> UB <math>\rightarrow</math> PE core Backward: UB <math>\rightarrow</math> PE core</li> <li>• <b>Reuse in PE core</b> Forward: Multiple times for convolutional reuse and for different samples of minibatch Backward: Multiple times to calculate the gradient of input/IFMAP</li> </ul>
	FC Layer: $n_{fc} \times m_{fc}$			Weights are double-buffered to PE core's SRAM to hide DRAM access latency	
Upstream gradient, gradient of loss function, gradient of activation function, optimizer states	Same as current layer's IFMAP and filter weights	Not Applicable (N/A)	<ul style="list-style-type: none"> <li>• <b>HBM3 DRAM</b> Read &amp; Write: None, if <math>UB \geq</math> all grad., else multiple*</li> <li>• <b>Unified Buffer (UB)</b> Read: UB <math>\rightarrow</math> PE core: Once* UB <math>\rightarrow</math> HBM3: None, if <math>UB \geq</math> all grad., else multiple* Write: PE <math>\rightarrow</math> UB: Once* HBM3 <math>\rightarrow</math> UB: None, if <math>UB \geq</math> all grad., else multiple*</li> </ul>	Not Applicable (N/A)	<ul style="list-style-type: none"> <li>• <b>Dataflow</b> PE core <math>\rightarrow</math> SRAM <math>\rightarrow</math> UB</li> <li>• <b>Reuse in PE core</b> For previous layer's gradient calculation</li> </ul>

\*Exact access count depends on UB size, batch-size, IFMAP & OFMAP size, PE core dimension, kernel size, number of filters, and dataflow mapping

$K - 1$  clock cycles and generates the output matrix,  $K \times N$ . Based on the above dataflow and mapping, the peak read-write bandwidth per clock cycle for different cases is summarized in Table 1. The expressions are shown for weight stationary dataflow. However, the above expressions hold for the output and input stationary dataflow, except the fixed and streamed matrix getting swapped.

### 3.2 Memory Access Patterns

Our proposed memory system consists of HBM3 (off-chip memory), a large Unified Buffer (UB) with multiple SOT-MRAM banks, a smaller double-buffered SRAM, and PE reg file specific to each PE unit (Fig. 3). The banks inside SOT-MRAM are optimized through a DTCO between the SOT-MRAM parameters and the workload requirements. The double-buffered SRAM holds the weights (during inference) and partial outputs. Its size is determined by the PE array size and the largest partial output size. In this subsection, we analyze the memory access patterns of CV and NLP models for the proposed memory system. The terms GLB and UB are used interchangeably in the paper to represent the large on-chip memory.

#### 3.2.1 CV models

Deep Residual Networks, having convolutional layers at their core, dominate the Computer Vision domain. The input

images are convolved with the layer-specific filter weights to produce the output feature map (OFMAP). The OFMAP goes through the pooling and normalization layers to act as input (IFMAP) to the next layer. The linear and softmax layer at the end finally recognizes the image (Fig. 4). The dimensionality of the key components of such models depends on the model architecture (Table 2 column 1 & 2). Depending on the UB size, activation & weight size, the minimum memory accesses requirement of each layer's activations and weights in different levels of memory hierarchy during inference and training are listed in col. 3 & 4 of Table 2, respectively. During inference, the read-only weights are directly loaded from HBM3 to the register file of each PE unit, bypassing the UB. However, we use double-buffered SRAM to hide the off-chip access latency. While the array is computing with loaded weights, the next set of weights is temporarily written to the SRAM buffer to hide the off-chip access latency behind the PE array computation latency. *Read: Once\** under heading HBM3 DRAM means the whole chunk of data, for example, *Initial Input(I)*, is read once from DRAM given that the Unified Buffer (UB) is large enough to hold all samples in the minibatch. *UB  $\rightarrow$  PE core* means the entity is read from UB and written into or operated inside PE core. We also provide a high-level dataflow and reuse scope for each entity during inference and training (col. 5 & 6 of Table 2, respectively). To illustrate, the last column of the



TABLE 3  
Architecture-and-platform-agnostic Memory access and Dataflow of Transformer-based NLP model workload during inference and training

Data Entity	Data Dimension	Memory Accesses		Dataflow & Reuse Status	
		Inference	Training	Inference	Training
Encoder Layer					
Input Sequence (I)	$N_{sql} \times N_{bt}$	<ul style="list-style-type: none"><li>• <b>HBM3 DRAM</b> Read: Once*, if <math>UB \geq I</math>, else multiple* Write: No write back</li><li>• <b>Unified Buffer (UB):</b> Read: UB <math>\rightarrow</math> PE core: Once* UB <math>\rightarrow</math> HBM3: None Write: PE core <math>\rightarrow</math> UB: None HBM3 <math>\rightarrow</math> UB: Once*, if <math>UB \geq I</math>, else multiple*</li></ul>	<ul style="list-style-type: none"><li>• <b>HBM3 DRAM</b> Read: Once*, if <math>UB \geq I</math>, else multiple* Write: No write back</li><li>• <b>Unified Buffer (UB):</b> Read: UB <math>\rightarrow</math> PE core: Twice*(one during forward pass, one during backward pass to calculate gradient) UB <math>\rightarrow</math> HBM3: None Write: PE core <math>\rightarrow</math> UB: None HBM3 <math>\rightarrow</math> UB: Once*, if <math>UB \geq I</math>, else multiple*</li></ul>	<ul style="list-style-type: none"><li>• <b>Dataflow</b> <math>HBM3 \rightarrow UB \rightarrow PE\ core</math></li><li>• <b>Reuse in PE core</b> No reuse</li></ul>	<ul style="list-style-type: none"><li>• <b>Dataflow</b> Forward: <math>HBM3 \rightarrow UB \rightarrow PE\ core</math> Backward: <math>UB \rightarrow PE\ core</math></li><li>• <b>Reuse in PE core</b> Forward &amp; backward pass: No reuse</li></ul>
Embedded Input	$N_{sql} \times N_{em} \times N_{bt}$	<ul style="list-style-type: none"><li>• <b>HBM3 DRAM</b> Read &amp; Write: None, if UB can hold full batch, else multiple*</li><li>• <b>Unified Buffer (UB):</b> Read: UB <math>\rightarrow</math> PE core: Once*, if PE array can produce complete output in one iteration, else multiple*</li></ul>	<ul style="list-style-type: none"><li>• <b>HBM3 DRAM</b> Read &amp; Write: None, if UB can hold full batch, else multiple*</li><li>• <b>Unified Buffer (UB):</b> Read: UB <math>\rightarrow</math> PE core: twice* (once at forward pass &amp; once at backward pass for local gradient calculation) UB <math>\rightarrow</math> HBM3: None, if UB can hold full batch, else multiple*</li></ul>	<ul style="list-style-type: none"><li>• <b>Dataflow</b> <math>PE\ core \rightarrow SRAM/UB</math></li><li>• <b>Reuse in PE core</b> As input to <math>Q</math>, <math>K</math>, and <math>V</math> layer for next stage</li></ul>	<ul style="list-style-type: none"><li>• <b>Dataflow</b> Forward: <math>PE\ core \rightarrow SRAM \rightarrow UB</math> Backward: <math>UB \rightarrow PE\ core</math></li><li>• <b>Reuse in PE core</b> Forward &amp; Backward pass: To calculate <math>Q</math>, <math>K</math>, and <math>V</math> layer activation and weight gradient</li></ul>
Query(Q), Key(K), Value(V), Output of Concat. Layer (Z), Output of Multi-head attention Layer (E)	$N_{sql} \times N_{em} \times N_{bt}$	<ul style="list-style-type: none"><li>• <b>HBM3 DRAM</b> Read: UB <math>\rightarrow</math> PE core: Once*, if PE array can produce complete output in one iteration, else multiple*</li></ul>	<ul style="list-style-type: none"><li>• <b>HBM3 DRAM</b> Read: UB <math>\rightarrow</math> PE core: twice* (once at forward pass &amp; once at backward pass for local gradient calculation) UB <math>\rightarrow</math> HBM3: None, if UB can hold full batch, else multiple*</li></ul>	<ul style="list-style-type: none"><li>• <b>Dataflow</b> <math>PE\ core \rightarrow SRAM/UB</math></li><li>• <b>Reuse in PE core</b> For next stage activation calculation</li></ul>	<ul style="list-style-type: none"><li>• <b>Dataflow</b> Forward: <math>PE\ core \rightarrow SRAM \rightarrow UB</math> Backward: <math>UB \rightarrow PE\ core</math></li><li>• <b>Reuse in PE core</b> Forward &amp; Backward pass: For next stage activation &amp; gradient calculation</li></ul>
Attention Filter (AF)	$N_{sql} \times N_{sql} \times N_{bt}$	<ul style="list-style-type: none"><li>• <b>HBM3 DRAM</b> Read: PE core <math>\rightarrow</math> UB: Once*, if PE array can produce complete output in one iteration, else multiple*</li></ul>	<ul style="list-style-type: none"><li>• <b>HBM3 DRAM</b> Read: PE core <math>\rightarrow</math> UB: Once* (during forward pass for next layer &amp; for future access in backprop) HBM3 <math>\rightarrow</math> UB: None, if UB can hold full batch, else multiple*</li></ul>	<ul style="list-style-type: none"><li>• <b>Dataflow</b> <math>PE\ core \rightarrow SRAM/UB</math></li><li>• <b>Reuse in PE core</b> As input to <math>K</math> &amp; <math>V</math> of Encoder-Decoder SelfAttention Layer</li></ul>	<ul style="list-style-type: none"><li>• <b>Dataflow</b> Forward: <math>PE\ core \rightarrow SRAM \rightarrow UB</math> Backward: <math>UB \rightarrow PE\ core</math></li><li>• <b>Reuse in PE core</b> Forward &amp; Backward pass: To find <math>K</math>, <math>V</math> and weight gradient of Encoder-Decoder Self-Attention Layer</li></ul>
Final Encoder Output Layer	$N_{sql} \times N_{em} \times N_{bt}$	<ul style="list-style-type: none"><li>• <b>HBM3 DRAM</b> Read: HBM3 <math>\rightarrow</math> UB: None, if UB can hold full batch, else multiple*</li><li>• <b>SRAM:</b> Multiple R/W for partial sums and local reuse</li></ul>	<ul style="list-style-type: none"><li>• <b>HBM3 DRAM</b> Read: HBM3 <math>\rightarrow</math> UB: None, if UB can hold full batch, else multiple*</li><li>• <b>SRAM:</b> Multiple R/W for partial sums and local reuse</li></ul>		
Upstream Gradient ( $\delta_x$ ) $x = 1, 2, 3, \dots, N$	Same as current layer activation	Not Applicable (N/A)	<ul style="list-style-type: none"><li>• <b>HBM3 DRAM</b> Read &amp; Write: None, if <math>UB \geq</math> all grad., else multiple*</li><li>• <b>Unified Buffer (UB):</b> Read: UB <math>\rightarrow</math> PE core: Once*, if PE core <math>\geq</math> all grad., else multiple*</li><li>• <b>SRAM:</b> Multiple R/W for partial sums and local reuse</li></ul>	Not Applicable (N/A)	<ul style="list-style-type: none"><li>• <b>Dataflow</b> <math>PE\ core \rightarrow SRAM \rightarrow UB</math></li><li>• <b>Reuse in PE core</b> For previous layer's <math>\delta</math> calculation</li></ul>
Gradient of Loss ( $\Delta L$ ) (only for final output layer)					
Gradient of activations					
Embedding Weights ( $W^{em}$ )	$N_{vocab} \times N_{em}$	<ul style="list-style-type: none"><li>• <b>HBM3 DRAM</b> Read: HBM3 <math>\rightarrow</math> PE core: Once*, if PE array can hold full weight matrix, else multiple*</li><li>• <b>Unified Buffer (UB)</b> Write: PE core <math>\rightarrow</math> HBM3: No write back</li><li>No read and write</li></ul>	<ul style="list-style-type: none"><li>• <b>HBM3 DRAM</b> Read: Once*, if <math>UB \geq W</math>, else multiple* Write: At least once* (to write back updated weights after training)</li><li>• <b>Unified Buffer (UB):</b> Read: UB <math>\rightarrow</math> PE core: at least thrice* (one at forward pass, two at backward pass to calculate <math>\Delta W</math> and updated <math>W</math>) UB <math>\rightarrow</math> HBM3: At least once* (to write back updated weights after training) Write: PE core <math>\rightarrow</math> UB: At least once* (to update weights) HBM3 <math>\rightarrow</math> UB: Once*, if <math>UB \geq W</math>, else multiple*</li><li>• <b>SRAM:</b> Multiple R/W for partial <math>W</math>, <math>\Delta W</math> per minibatch iteration to facilitate reuse</li></ul>	<ul style="list-style-type: none"><li>• <b>Dataflow</b> <math>HBM3 \rightarrow PE\ core/SRAM</math></li><li>• <b>Reuse in PE core</b> Multiple times for each sample per minibatch</li></ul>	<ul style="list-style-type: none"><li>• <b>Dataflow</b> Forward: <math>HBM3 \rightarrow UB \rightarrow PE\ core</math> Backward: <math>UB \rightarrow PE\ core</math></li><li>• <b>Reuse in PE core</b> Forward: Multiple times for each sample per minibatch Backward: For next stage gradient calculation</li></ul>
Query Weights ( $W^Q$ )	$(N_{em} \times d_q) * h$				
Key Weights ( $W^K$ )	$(N_{em} \times d_k) * h$				
Value Weights ( $W^V$ )	$(N_{em} \times d_v) * h$				
Concat. Weights ( $W^O$ )	$N_{em} \times N_{em}$				
FFN FC1 Weights ( $W^{FC1}$ )	$N_{em} \times d_{ff}$				
FFN FC2 Weights ( $W^{FC2}$ )	$d_{ff} \times N_{em}$				
Output classifier weights ( $W^{cl}$ )	$(N_{sql} * N_{em}) \times N_{vocab}$				
Optimizer states		Not Applicable (N/A)	<ul style="list-style-type: none"><li>• <b>HBM3 DRAM</b> Read &amp; Write: None</li><li>• <b>Unified Buffer (UB)</b> Read: <math>UB \rightarrow PE\ core</math>: Once*</li><li>Write: <math>PE\ core \rightarrow UB</math>: Once*</li><li>• <b>SRAM</b> Read &amp; Write: None</li></ul>	Not Applicable (N/A)	<ul style="list-style-type: none"><li>• <b>Dataflow</b> <math>UB \rightarrow PE\ core</math></li><li>• <b>Reuse in PE core</b> No reuse</li></ul>
Decoder Layer					
The decoder layer has two multi-head attention layers; (i) Decoder self-attention layer and (ii) Encoder-Decoder attention layer. Each of them has similar data entities ( $Q$ , $K$ , $V$ , $Z$ , $E$ , $AF$ , $W^Q$ , $W^K$ , $W^V$ , $W^O$ ) and $W^{FC1}$ , $W^{FC2}$ with same dimension. However, the sequence length might vary from that of the Encoder's one.					

The decoder layer has two multi-head attention layers; (i) Decoder self-attention layer and (ii) Encoder-Decoder attention layer. Each of them has similar data entities ( $Q$ ,  $K$ ,  $V$ ,  $Z$ ,  $E$ ,  $AF$ ,  $W^Q$ ,  $W^K$ ,  $W^V$ ,  $W^O$ ) and  $W^{FC1}$ ,  $W^{FC2}$  with same dimension. However, the sequence length might vary from that of the Encoder's one.

\*Exact access count depends on UB size, weight matrix, PE core dimension, and dataflow mapping

first row indicates input images' dataflow and reuse status during training. During the forward pass, input images are read from HBM3, written to UB, and read from UB to be operated inside PEs core. For weight gradient calculation, the inputs are read from UB to PE core during backpropagation, assuming that the UB is large enough to hold the input images along with the generated ofmap of the current layer, thus avoiding the DRAM accesses during backward pass. *Reuse in PE core* represents at forward pass, the inputs can be reused multiple times for convolutional and filter reuse. It can also be reused multiple times during backpropagation to calculate the gradients of different filters. Row 5 of Table 2 shows the training-specific ephemeral entities with their dimension, memory access count, and reuse status. The training workflow is complicated and requires many more

memory accesses (both off-chip and on-chip) compared to inference. For example, to calculate the weight gradients of Layer 1, it requires the current layer's activation gradient  $\frac{da_1}{dz_1}$ , input ( $a_0$ ), next layer's weight ( $W_2$ ) and the upstream gradient from Layer 2 ( $\delta_1$ ) (as shown in Fig. 5).

### 3.2.2 Natural Language Processing (NLP)

We analyze the state-of-the-art Transformer model [18] as the representative of the NLP domain. The input sequence propagates through the embedding layer and different sublayers of the encoder stacks to extract different linguistic features and inter-token dependency of the input sequence. The decoder stacks then generate the output sequence by taking the encoded input sequence from the encoder stack and the output sequence generated by itself in the

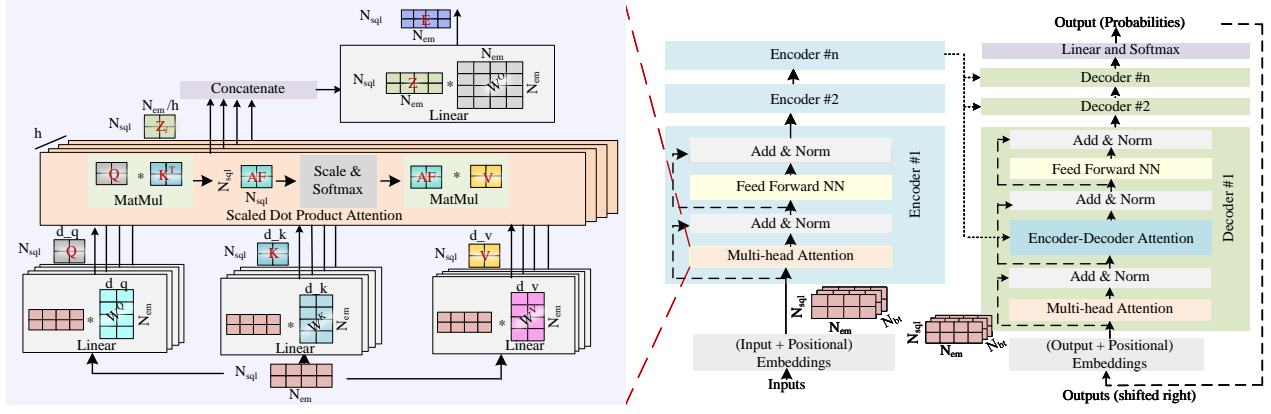


Fig. 6. Transformer model workflow breakdown

previous timesteps (Fig 6). The input sequence multiplied by different layer weights takes different activation names and shapes (Table 3 col. 1 & 2) throughout the model operation. We summarize the minimum memory accesses requirement, dataflow and reuse scopes of each layer's (sub-layer) activations and weights in different levels of memory hierarchy during inference and training are in Table 3. We follow the same convention as Table 2. We illustrate one cell of Table 3 to help the readers navigate the table. The last column of the second row indicates the dataflow and reuse status of Embedded input during training. During forward pass, the embedded inputs are generated inside the PE core, partial sums are accumulated in the SRAM, and finally, the output is written to Unified buffer (UB). For weight gradient calculation, the embedded inputs are read from UB to PE core during backpropagation. *Reuse inside PE core* represents at forward pass, the embedded input can be reused thrice as input to Key, Query, and Value linear layer. It can also be reused thrice during backpropagation to calculate the weight gradient of the Key, Query, and Value linear layer.

We consider the memory access counts in terms of how many times the data entities operate throughout the workflow. However, the exact access count depends on the model architecture, hyperparameters, hardware platforms, dataflow & mapping such as IFMAP, OFMAP, word embedding, input sequence length, weight size, batch size, UB size, SRAM size, PE core dimension, row-stationary dataflow, etc.

## 4 DTCO OF SOT-MRAM

An efficient memory system is required to ensure the overall system performance for Deep Learning workloads. The memory system should have large on-chip memory to avoid frequent DRAM accesses, and the on-chip memory should have high bandwidth to prevent the system from being memory-bound while being energy efficient. In this section, we perform a DTCO of SOT-MRAM in bit-cell level based on the workload profiling done in section 3.

### 4.1 Optimizing critical switching current $I_c$

In SOT-MRAM, the magnetic orientation of the free layer is switched by Spin-Orbit Torque (SOT) induced by spin Hall and interfacial effects between the channel and free layer

(FL) of MTJ. An in-plane charge current is flown through the channel (also known as Spin Hall or SOT layer) to generate a spin current that exerts a spin torque on the free layer. When this spin torque becomes strong enough, it rotates the free layer's magnetic orientation. From the macrospin model, the critical current density required to switch the magnetic orientation of FL is expressed as [21]

$$j_c = \frac{2e\mu_0 M_{s,FL} t_{FL}}{\hbar \theta_{SH}} \left( \frac{H_{k,eff}}{2} - \frac{H_x}{\sqrt{2}} \right) \quad (9)$$

Where  $H_{k,eff}$  is the effective anisotropy field,  $H_x$  is the applied field,  $M_{s,FL}$  is the saturation magnetization of free layer, and  $t_{FL}$  is its thickness. Our interest is in lowering the switching current to achieve low write energy. Here, the free layer thickness  $t_{FL}$  and spin Hall efficiency  $\theta_{SH}$  act as a control knob for critical switching current.  $\theta_{SH}$  is a material-specific parameter and its higher value is expected to reduce the switching current. The typical value of  $\theta_{SH}$  in heavy metal alloys ranges between 0.1 to 0.5 [20]. However, recent topological insulators as SOT layer can have a very large  $\theta_{SH}$ . [22] demonstrated  $\theta_{SH} = 152$  with *BiSb* thin films.

## 4.2 Optimizing read-write pulse width

### 4.2.1 Read pulse width

The reading of SOT-MRAM involves sensing the resistance status of the MTJ. A small amount of current  $I_{data}$  is passed through the MTJ stack. The voltage drop across the stack  $V_{data+}$  or  $V_{data-}$  is compared against a reference voltage  $V_{ref} = \frac{1}{2}(V_{data+} + V_{data-})$  to read out the stored bit. The read Sensing Margin  $SM = |V_{ref} - V_{data}|$  is typically very small (in 100s of nV range). Sensing and amplifying this small difference requires a strong and complex Sense Amplifier (SA) that contributes to most of the read latency and energy. The SM is determined by the Tunnel Magneto Resistance ratio ( $TMR\ ratio = \frac{R_{AP} - R_P}{R_P}$ ) of MTJ. A higher TMR ratio produces a larger SM by making  $V_{data+}$  higher and  $V_{data-}$  lower. Thus the TMR ratio is inversely proportional to the read latency [23]. The higher the TMR window, the higher the read speed and the less effort required on the periphery. The typical range of the TMR ratio is between 100 to 300%. The TMR is tunable by oxide thickness [24] as shown in Fig. 15 (a). In SOT-MRAM, we can increase the oxide thickness, thanks to the decoupled read-write path of SOT-MRAM, to

achieve a high TMR and increase the read speed without worrying about the large incubation time in STT-MRAM stemming from the thick oxide barrier. A thick oxide barrier also prevents time-induced wear out of the MTJ stack [25].

TABLE 4  
DTCO control parameters & their impact on Power, Performance and Area (PPA)

DTCO Parameters	Impact on PPA
Spin Hall angle $\theta_{SH}$	$\theta_{SH} \uparrow$ , $j_c \downarrow$ , Switching energy $\downarrow$
Free layer thickness $t_{FL}$	$t_{FL} \downarrow$ , $j_c \downarrow$ , Switching energy $\downarrow$ , Area $\downarrow$
SOT layer dimension $A_{SOT}$	$A_{SOT} \downarrow$ , $\tau_p \downarrow$ , Area $\downarrow$ , Write Bandwidth $\uparrow$
Oxide thickness $t_{MgO}$	$t_{MgO} \uparrow$ , TMR $\uparrow$ , Read Bandwidth $\uparrow$

#### 4.2.2 Write pulse width $\tau_p$

The width of the write current pulse for switching is inversely proportional to the magnitude of the applied current density in the SOT layer  $j_{sw}$  [20]

$$\tau_p \propto \frac{1}{j_{sw}} \quad (10)$$

As the area of the SOT layer ( $A_{SOT}$ ) is scaled down, the effective current density increases,  $j_{sw} \propto 1/(A_{SOT})$ . Successful switching should take place when  $j_{sw} > j_c$ . We can increase  $j_{sw}$  by reducing the SOT layer dimension and decrease  $j_c$  by increasing  $\theta_{SH}$  or by decreasing  $t_{FL}$ . Thus we can achieve successful switching in much shorter pulse width (equation 10). [26] demonstrated the switching at 180ps, [27] at 400ps, and [28] at 210ps. Switching in shorter pulse width ensures larger write bandwidth which is essential for memory systems used in AI/Deep Learning hardware. The key DTCO parameters of SOT-MRAM and their impact on Power, Performance and Area (PPA) are listed in Table 4.

## 5 RESULTS AND ANALYSIS

In this section, we provide the result and analysis of the STCO on the CV and NLP workloads during inference and training and present the optimum Power, Performance, and Area results by performing the DTCO of SOT-MRAM. We developed a MATLAB-based framework to implement our analytical *Memory and Compute Model*. Unlike ScaleSim [29] and Timelooop [30] simulator, which only support profiling DNN workloads in inference mode to date, our model captures both training and inference behavior of CV and NLP models.

### 5.1 Bandwidth Demand

In Fig. 7 (a), (b), we plot the read-write on-chip bandwidth demand in *bytes/cycle* of 18 widely used CV models. Resenet101 and Resnet50 running on a 256×256 PE array will demand the highest read bandwidth, 4017 bytes/cycle, from GLB, whereas Squeezenet will demand the lowest bandwidth, 1028 bytes/cycle. Naturally, as the PE array size increases, the computation capacity per cycle  $T_{MAC}$  increases which demands more data from memory to keep all PEs active. From the workload perspective, we observe that the most contributing factor to the read bandwidth demand is its inverse relationship with the filter and ofmap size. We explain the inverse relationship of filter and ofmap size with

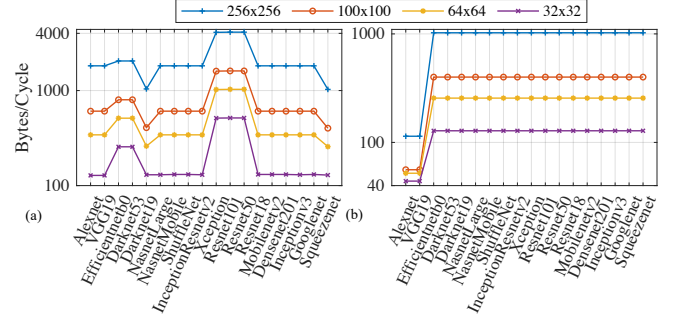


Fig. 7. Bandwidth requirement of CV models for different PE array size. (a) Read Bandwidth, (b) Write Bandwidth.

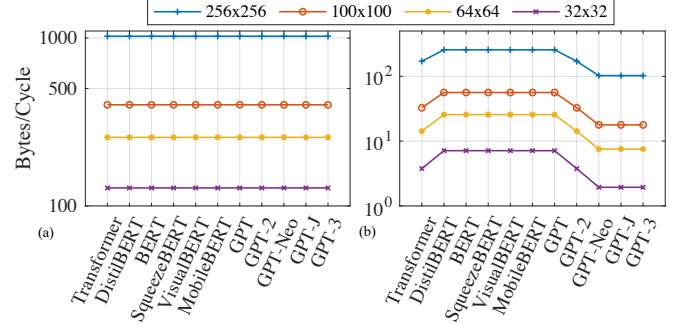


Fig. 8. Bandwidth requirement of NLP models for different PE array size. (a) Read Bandwidth, (b) Write Bandwidth.

the read bandwidth using the convolutional reuse concept. As the filter size decreases, the scope of convolutional reuse decreases. The ofmap again depends on the filter and ifmap size. With the decrease of filter size and ofmap size, the convolutional reuse decreases, giving rise to more bandwidth demand. The layer of Resnet101 that requires the most bandwidth (4017 bytes/cycle) has the ofmap dimension (7×7) and filter dimension (1×1). On the other hand, the most demanding (1028 bytes/cycle) layer of Squeezenet has the ofmap dimension (18×18) and filter dimension (1×1). Another observation is that though 1×1 convolution reduces the computation complexity, it requires more bandwidth from memory, i.e., becomes memory intensive.

The write bandwidth is also inversely proportional to the filter size. However, in 1×1 convolutions, it depends on the number of outputs generated by the PE array. The write bandwidth is always smaller than the read bandwidth (Fig. 7 (b)) as it takes more than one operand to generate one output. For example, in a 3×3 convolution, it takes 18 operands to generate a single output; in a 1×1 convolution, it takes two operands to generate one output element.

In transformer-based NLP models, the computations are essentially the GEMM operation. The bandwidth estimation of these models is performed using the same expressions as FC layers. As the dimension of the operand matrices is larger than the PE array dimension, following case iv (Table 1, section 3.1.3), the read bandwidth of all models depends on the PE array size (Fig. 8 (a)). The write bandwidth depends on the PE array dimension and the input sequence length. As different models are trained with different input sequence lengths [31], their write bandwidth demand is not the same



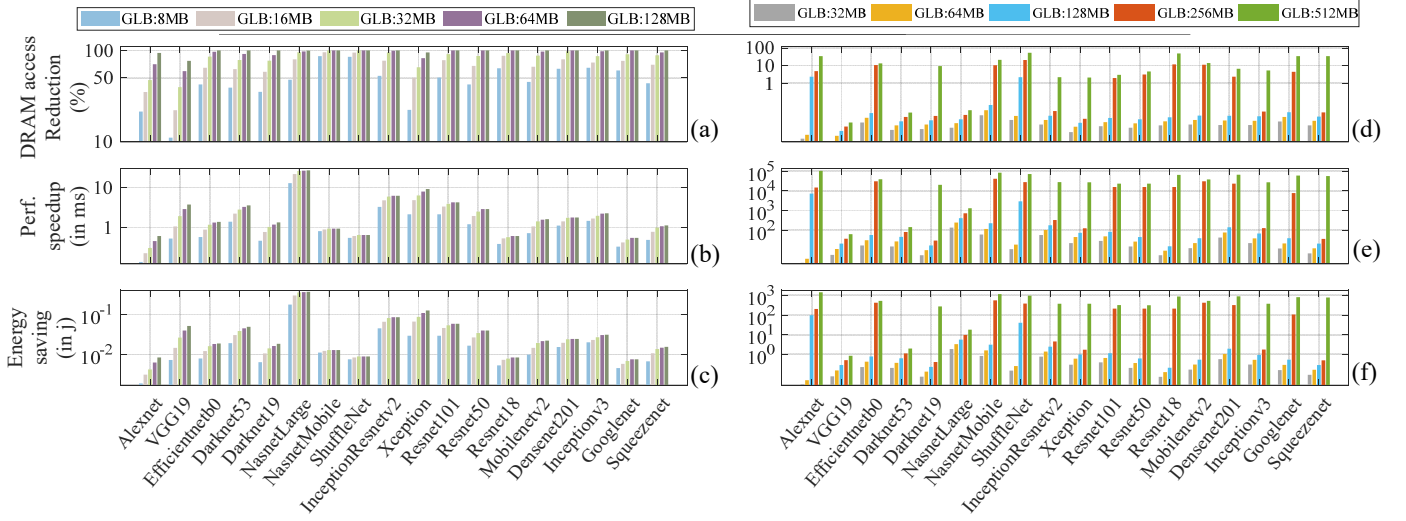


Fig. 9. Impact of larger GLB memories on performance and energy efficiency for CV models at inference and training. Percentage reduction in DRAM accesses at inference (a) and training (d). Performance Speedup from DRAM access reductions at inference (b) and training (e). Energy savings from reduced DRAM accesses at inference (c) and training (f). Both cases compare results to a baseline of 2MB GLB running 16 samples.

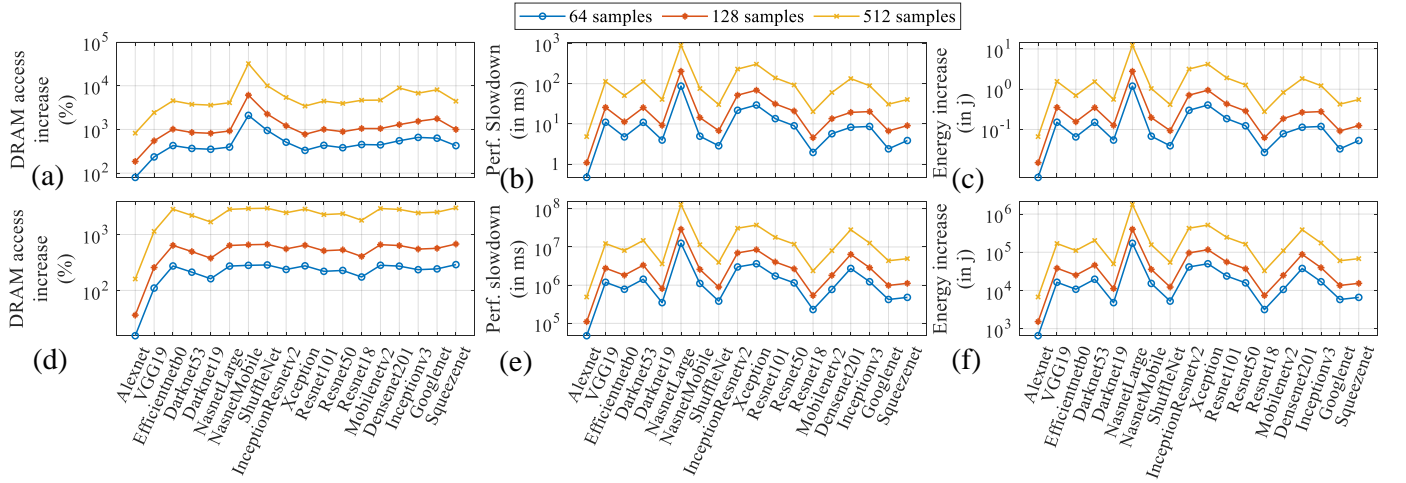


Fig. 10. Impact of batch size on performance and energy efficiency for CV models at inference and training. Percentage increase in DRAM accesses at inference (a), at training (d). Performance slowdown (latency increase) from extra DRAM accesses at inference (b), at training (e). Energy increase from extra DRAM accesses at inference (c), at training (f). In both cases, results are compared to a baseline of 16 samples running with 4MB GLB.

across all models. The models having the highest sequence length (2048) have the lower write bandwidth demand 102 bytes/cycle running on a  $256 \times 256$  PE array (Fig. 8 (b)).

## 5.2 Impact of on-chip memory

Compared to a GLB size of 2MB, the DRAM access counts for all CV models decrease significantly if we increase the GLB size. In inference, reaching the 100% reduction in access means it only needs to read the initial inputs, weights for each layer, and write the final layer output, no DRAM access is needed for the intra and inter-layer operations. Further increase in GLB size will not positively impact the performance in these cases. For 16 samples, DRAM access is reduced by 100% for 14 models at 128MB, and most models experience a reduction of >80% at 64MB (Fig. 9 (a)). Fig. 9 (b), (c) show the performance speedup and energy saving coming from these DRAM access reductions.

We observe a slower improvement in the DRAM access reduction during training unless the GLB size is large enough, at least 256MB for most models (Fig. 9 (d)). However, even the smaller percent reduction in DRAM access results in significant performance and energy improvement (Fig. 9 (e), (f)). This is because training requires at least  $2 \times$  DRAM accesses as inference. A similar trend is observed for NLP models. Transformer-based NLP models are usually larger than the CV models. This is the reason we achieve more performance speedup and energy reduction even at smaller DRAM access reduction rate (see Fig. 11).

We also observe the impact of batch size on the system performance. DNN models learn faster if we increase the batch size. Thus for a fixed GLB size, the DRAM access count increases significantly at larger batch size, causing performance slowdown and more energy consumption. Fig. 10 and Fig. 12 (a, b, c for inference and d, e, f for training) show the increase in DRAM access count and its associated

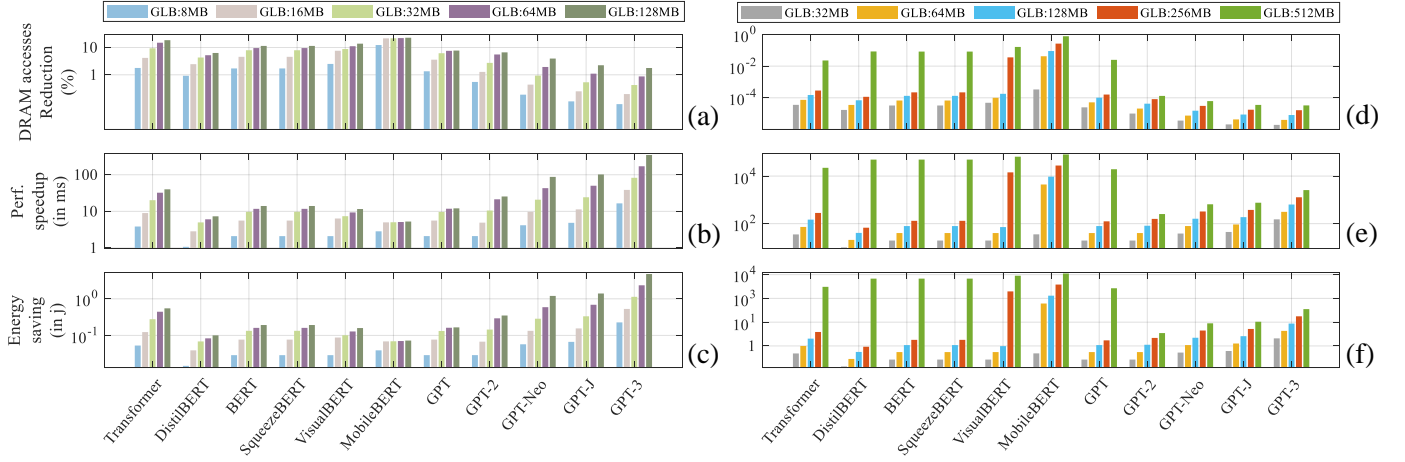


Fig. 11. Impact of larger GLB memories on performance and energy efficiency for NLP models at inference and training. Percentage reduction in DRAM accesses at inference (a), at training (d). Performance Speedup from DRAM access reductions at inference (b), at training (e). Energy savings from reduced DRAM accesses at inference (c), at training (e). In both cases, results are compared to a baseline of 2MB GLB running 16 samples

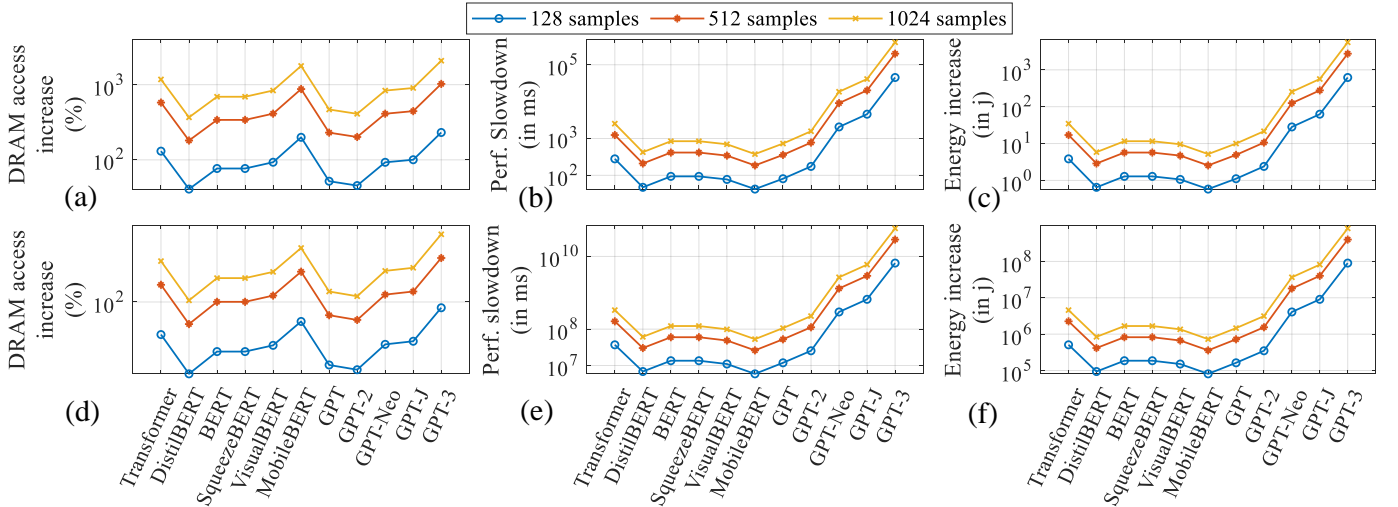


Fig. 12. Impact of batch size on performance and energy efficiency for NLP models at inference and training. Percentage increase in DRAM accesses, inference (a), and training (d). Performance slowdown (latency increase) from extra DRAM accesses at inference (b), at training (e). Energy increase from extra DRAM accesses at inference (c), at training (f). Results are compared to a baseline of 16 samples running with 4MB GLB.

impact on performance and energy for CV and NLP models respectively at different batch sizes.

The key takeaway from this analysis is that we can reduce the energy and latency associated with DRAM accesses if we increase the GLB size. For larger batch sizes, the energy and latency improvement is even more.

### 5.3 DTCO of SOT for PPA Optimization

From section 5.2 we see that the GLB size of 64MB (for inference) and 256MB (for training) offer significant energy and performance improvement. However, it is not feasible and efficient to use such large SRAMs because of its area and leakage power, even if the low-power techniques are employed. Section 5.1 implies that we need approximately 4000bytes/cycle bandwidth between GLB and PE array for larger array size (256×256). In this subsection, we provide the SOT-MRAM DTCO results and observation meeting the requirements stated in the above two subsections. We perform the DTCO in *Cadence Virtuoso* tool using the compact

SOT-MRAM model from [15], and use *Synopsys* 14nm library [33] for the CMOS transistors and peripheral circuits.

#### 5.3.1 $I_c$ optimization

To realize the impact of SOT efficiency  $\theta_{SH}$  on  $I_c$ , we sweep  $\theta_{SH}$  from 0.1 to 100 (Fig. 13 (a)). With  $\theta_{SH} \geq 100$ ,  $I_c$  goes as low as 0.5uA. Even though the widely used SOT layers are made of heavy metal alloys having smaller  $\theta_{SH}$  (e.g., 0.1 to 0.5), recent advancement in material engineering demonstrates that in topological insulator  $\theta_{SH}$  can go as high as 152 [22]. We recommend using topological insulators as the SOT layer to achieve a lower switching current.

Next, we analyze the impact of SOT layer geometry on the switching current (Fig. 13 (b), (c)).  $I_c$  scales down linearly with the decrease of SOT layer width, and  $w_{SOT}$  can be set to desired value based on the performance and reliability requirement (Fig. 13 (b)). While  $I_c$  scales linearly with the width of the SOT layer, the thickness of the SOT layer has an interesting effect on the switching current. The SOT layer

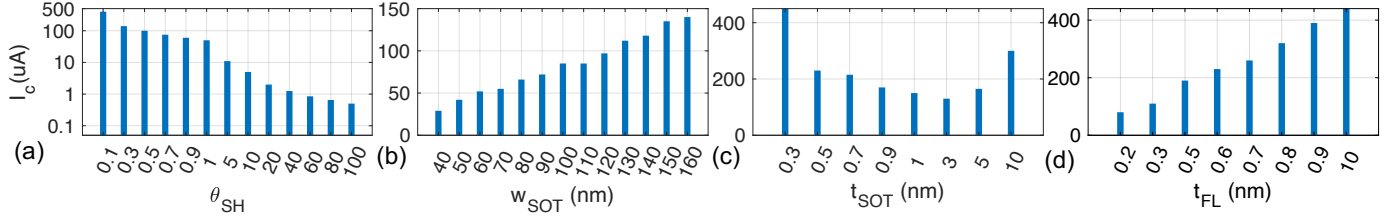


Fig. 13. Critical current vs  $\theta_{SH}$ (a),  $w_{SOT}$ (b),  $t_{SOT}$ (c), and  $t_{FL}$ (d).

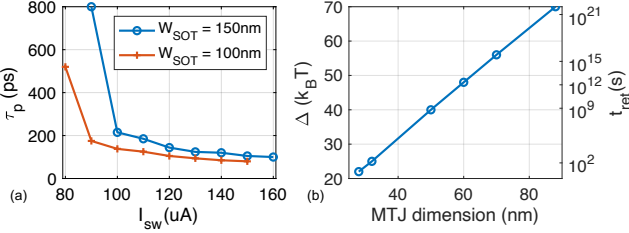


Fig. 14. (a) Switching pulse width  $\tau_p$  vs applied switching current  $I_{sw}$ . (b) Thermal stability factor  $\Delta$  (left Y-axis) and retention time  $t_{ret}$  (right Y-axis) vs MTJ dimension for a fixed retention failure rate,  $P_{RF} = 10^{-9}$ . At  $\Delta = 70$ , MTJ dimension = 88nm, retention time is  $> 10$  years [32].

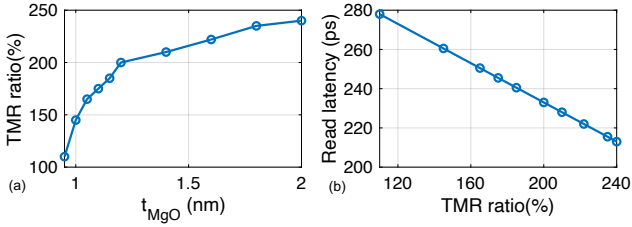


Fig. 15. (a) Impact of oxide thickness on TMR. (b) Impact of TMR on read latency.

should be relatively thin but bulk enough for heavy metal layers to experience the bulk effect to achieve high SOT efficiency. Once it crosses optimum thickness, which is 3nm (Fig. 13 (c)), many of the charges that are injected into the metal do not contribute to the switching. As a result,  $I_c$  goes high beyond 3nm of thickness.

The free layer thickness is a major contributor to optimizing the switching current. The smaller the thickness, the smaller the switching current (fig 13 (d)). However, with the scaling down of  $t_{FL}$ , the thermal stability factor  $\Delta$  also scales down, reducing the memory's data retention time  $t_{ret}$ . Non-volatility is a great feature of MRAM, but it can be compromised to achieve higher density, higher bandwidth, and lower energy when the target application is a cache. Because, in the cache even for AI workloads, the data lifetime is much shorter, typically in the seconds range [34]. Fig. 14(b) shows  $\Delta$  and  $t_{ret}$  as functions of free layer volume. While scaling down  $t_{FL}$  to optimize  $I_c$ , we keep an eye on the reliability of the stored data. We consider a retention failure rate of  $10^{-9}$  (i.e., 1 bit flip per billion) to adjust the  $t_{FL}$ .

### 5.3.2 Bandwidth optimization

As shown in Fig. 15 (a), [24] demonstrated that TMR ratio of the MTJ device can be increased by increasing the oxide thickness. We increase the oxide thickness from 1nm to

2nm to decrease the read latency from 260ps to 213ps (Fig. 15 (b)). The write pulse width is inversely proportional to the applied switching current. While we want to lower the applied current to achieve low energy, the higher amplitude of the applied current is required for faster magnetization reversal. However, switching occurs at smaller pulse width at the iso-current if we scale down the SOT layer width. This is because of the smaller critical current at smaller geometry (Fig. 13 (b,d)). Fig. 14(a) shows that switching pulse width is reduced significantly from 800ps to 175ps @90uA by scaling down the SOT layer width from 150nm to 100nm. Thus, we achieve higher write bandwidth by scaling down the SOT layer width to meet the high BW demand from AI workloads. The DTCO optimized parameters of SOT-MRAM used in this study are listed in Table 5.

TABLE 5  
SOT-MRAM DTCO optimized parameters

Parameter	Value	Parameter	Value
Spin Hall angle $\theta_{SH}$	1	TMR	240%
Free layer thickness $t_{FL}$	0.2nm	MTJ diameter	50nm
SOT width $w_{SOT}$	100nm	SOT thickness $t_{SOT}$	3nm
Oxide thickness $t_{MgO}$	2nm	Thermal stability factor $\Delta$	40

With a read latency of 213ps and a write latency of 175ps, each SOT-MRAM bit-cell can achieve a read bandwidth of 4.69Gbps and a write bandwidth of 5.71Gbps. We then dynamically allocate the memory bus width on-demand to satisfy the bandwidth requirement for different workloads and PE array size stated in section 5.1.

### 5.4 System level performance evaluation

In this subsection, we analyze the PPA metrics in the system level on the DNN benchmarks with SRAM, SOT-MRAM, and DTCO-optimized-SOT-MRAM. We simulate Synopsys 14nm low-power SRAM [33], and SOT-MRAM [15] in bit-cell level in Cadence Virtuoso and feed this data to Destiny [35] to find the array-level PPA. Destiny currently does not support SOT-MRAM; we modified the STT-MRAM source files to reflect the separate read-write path and SOT switching mechanism to incorporate SOT-MRAM. Based on the array-level results from Destiny, we estimate the system-level PPA metrics using our analytical model. This analysis only incorporates the PPA metrics from the memory system (DRAM and GLB) assuming that the PPA of the compute unit is constant. With SOT-MRAM as GLB, we observe significant energy and latency improvement over SRAM at 64MB (for inference) and 256MB (for training) (see Fig. 16 (a-d) for CV benchmarks and (e-h) for NLP benchmarks). On average, the 64MB SOT-MRAM offers 5 $\times$  energy reduction and 2 $\times$  latency reduction over 64MB SRAM across all CV models in inference

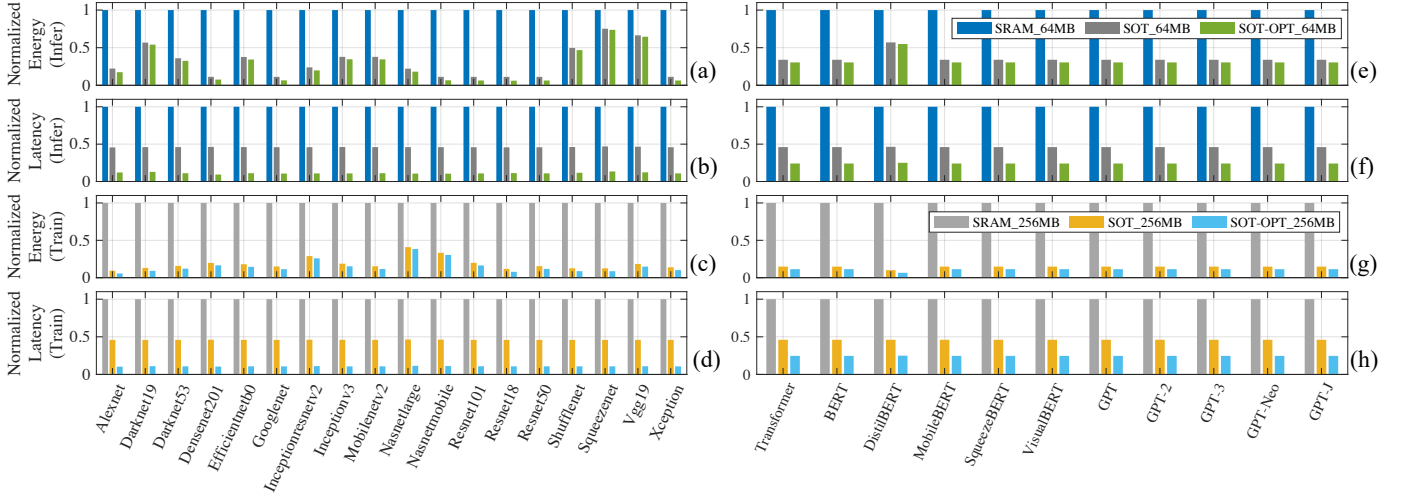


Fig. 16. System level energy improvement with SOT-MRAM and DTCTO-optimized-SOT-MRAM over SRAM at the same size for CV (a-d) and NLP (e-h) models. The top plots show energy (a, e) and latency (b, f) for inference, and the bottom plots show energy (c, g) and latency (d, h) for training.

mode. Our DTCTO-optimized-SOT-MRAM offers further improvement,  $7\times$  energy, and  $8\times$  latency reduction over SRAM at iso-capacity. We observe that the most contributing factor in energy reduction ( $>50\%$ ) is the near-zero leakage power of SOT-MRAM compared to high leakage power of SRAM. The improvement is even more in training mode;  $6\times$  ( $8\times$  with SOT-opt.) energy reduction and  $2\times$  ( $9\times$  with SOT-opt.) latency reduction. With 64MB SOT-MRAM, NLP models in inference mode experience  $2\times$  ( $3\times$  with SOT-opt.) energy reduction and  $2\times$  ( $4\times$  with SOT-opt.) latency reduction than 64MB SRAM. Like CV benchmarks, with 256MB SOT-MRAM, NLP benchmarks also experience more energy improvement,  $6\times$  ( $8\times$  with SOT-opt.), and latency improvement,  $2.5\times$  ( $4.5\times$  with SOT-opt.), in training mode. The more improvement in training mode is because of two reasons: (1) GLB size increases from 64MB to 256MB, and (ii) GLB access counts are significantly large (at least  $5\times$ ) in training. Our DTCTO-opt-SOT-MRAM further adds value to PPA by its smaller silicon area,  $0.54\times$  at 64MB and  $0.52\times$  at 256MB of 14nm SRAM at iso-capacity (Fig. 17).

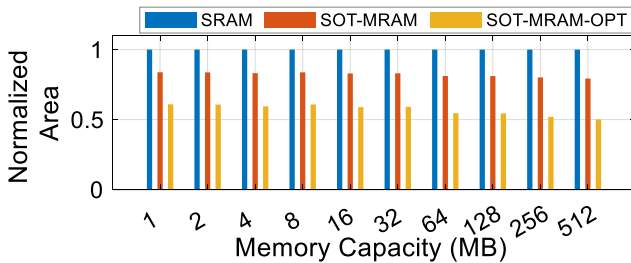


Fig. 17. Area improvement of SOT-MRAM and SOT-MRAM-OPT over SRAM

## 6 RELATED WORK

SOT-MRAMs have been widely studied as the next generation of STT-MRAM to leverage all benefits of MRAMs as embedded memory [9] [10] [12] [13] [16] [17]. However, very few studies have evaluated the performance of SOT-MRAM as on-chip memory in system-level. [14] and [36]

demonstrated the performance improvement of SOT-MRAM as L2 data cache compared to SRAM L2 cache on MiBench, SPEC2000 and SPEC2006 benchmarks. SOT-MRAMs have also been explored in the context of DL accelerators as a promising technology for In-Memory Computing (IMC) [37] [38] [39]. IMC has pros and cons, and our work where we use SOT-MRAM as the cache storage element differs from IMC. While the scope of SOT-MRAM has been explored both as regular CPU cache and IMC for DL accelerator to some extent, to the best of our knowledge, unlike IMC, this is the first work that presents a comprehensive analysis of SOT-MRAM as on-chip memory for application in AI/DL accelerators.

## 7 CONCLUSION

We proposed an efficient and high-performance memory system with SOT-MRAM for AI accelerators in this work. Guided by detailed target workload characterization, our memory system comprises of HBM3 DRAM, a DTCTO-enabled SOT-MRAM GLB and a small SRAM buffer. Our large SOT-MRAM GLB significantly reduces the energy and latency by reducing expensive DRAM accesses while still having acceptable on-chip access energy and latency, achieving overall system-level high performance. We finally demonstrate that our memory system performs  $8\times$  and  $9\times$  better in terms of energy and latency respectively on CV benchmarks in training (7 and 8 times better in inference) and  $8\times$  and  $4.5\times$  better in terms of energy and latency respectively on NLP benchmarks in training (3 and 4 times better in inference) while consuming only around 50% of SRAM area at iso-capacity.

## REFERENCES

- [1] J. Hestness, N. Ardalani, and G. Diamos, "Beyond human-level accuracy: Computational challenges in deep learning," in *Proceedings of the 24th Symposium on Principles and Practice of Parallel Programming*, ser. PPOPP '19, 2019, p. 1–14.
- [2] V. Sze, Y.-H. Chen, T.-J. Yang, and J. S. Emer, "Efficient processing of deep neural networks: A tutorial and survey," *Proceedings of the IEEE*, vol. 105, no. 12, pp. 2295–2329, 2017.



- [3] N. Jouppi et al., "A Domain-Specific Architecture for Deep Neural Networks," ACM Communications, 2018.
- [4] "NVIDIA Ampere100 GPU." [Online]. Available: <https://www.nvidia.com/en-us/data-center/ampere-architecture/>
- [5] Q. Cao et al., "Are mobile dnn accelerators accelerating dnn?" in *Proceedings of the 5th International Workshop on Embedded and Mobile Deep Learning*, 2021, pp. 7–12.
- [6] J. Park et al., "Deep learning inference in facebook data centers: Characterization, performance optimizations and hardware implications," *arXiv preprint arXiv:1811.09886*, 2018.
- [7] H.-S. P. Wong et al., "Stanford Memory Trends," 2020. [Online]. Available: <https://nano.stanford.edu/stanford-memory-trends>
- [8] H. Li, M. Bhargav, P. N. Whatmough, and H. Philip Wong, "On-Chip Memory Technology Design Space Explorations for Mobile Deep Neural Network Accelerators," in *Design Automation Conference (DAC)*, 2019.
- [9] T. Endoh, H. Honjo, K. Nishioka, and S. Ikeda, "Recent progresses in stt-mram and sot-mram for next generation mram," in *2020 IEEE Symposium on VLSI Technology*, 2020, pp. 1–2.
- [10] M. Gupta et al., "High-density sot-mram technology and design specifications for the embedded domain at 5nm node," in *2020 IEEE International Electron Devices Meeting*, 2020, pp. 24.5.1–24.5.4.
- [11] A.V. Khvalkovskiy et al., "Basic principles of STT-MRAM cell operation in memory arrays," in *Journal of Physics D: Applied Physics*, 2013.
- [12] M. Natsui et al., "Dual-port field-free sot-mram achieving 90-mhz read and 60-mhz write operations under 55-nm cmos technology and 1.2-v supply voltage," in *IEEE Symposium on VLSI Circuits*, 2020.
- [13] K. Garello, F. Yasin, and G. S. Kar, "Spin-orbit torque mram for ultrafast embedded memories: from fundamentals to large scale technology integration," in *2019 IEEE 11th International Memory Workshop (IMW)*, 2019, pp. 1–4.
- [14] F. Oboril, R. Bishnoi, M. Ebrahimi, and M. B. Tahoori, "Evaluation of hybrid memory technologies using sot-mram for on-chip cache hierarchy," *IEEE Transactions on Computer-Aided Design of Integrated Circuits and Systems*, vol. 34, no. 3, pp. 367–380, 2015.
- [15] M. Kazemi et al., "Compact model for spin-orbit magnetic tunnel junctions," *IEEE Transactions on Electron Devices*, vol. 63, no. 2, pp. 848–855, 2016.
- [16] S.Z. Rahaman et al., "Size-dependent switching properties of spin-orbit torque mram with manufacturing-friendly 8-inch wafer-level uniformity," *IEEE Journal of the Electron Devices Society*, vol. 8, pp. 163–169, 2020.
- [17] H. Honjo et al., "First demonstration of field-free sot-mram with 0.35 ns write speed and 70 thermal stability under 400°C thermal tolerance by canted sot structure and its advanced patterning/sot channel technology," in *2019 IEEE International Electron Devices Meeting (IEDM)*, 2019, pp. 28.5.1–28.5.4.
- [18] A. Vaswani et al., "Attention is all you need," *Advances in neural information processing systems*, vol. 30, 2017.
- [19] Y. Chen, T. Krishna, J. S. Emer, and V. Sze, "Eyeriss: An Energy-Efficient Reconfigurable Accelerator for Deep Convolutional Neural Networks," in *IEEE JSSC*, 2017.
- [20] A. Manchonet et al., "Current-induced spin-orbit torques in ferromagnetic and antiferromagnetic systems," *Reviews of Modern Physics*, vol. 91, no. 3, p. 035004, 2019.
- [21] K.-S. Lee, S.-W. Lee, B.-C. Min, and K.-J. Lee, "Threshold current for switching of a perpendicular magnetic layer induced by spin hall effect," *Applied Physics Letters*, vol. 102, no. 11, p. 112410, 2013.
- [22] N. H. D. Khang, Y. Ueda, and P. N. Hai, "A conductive topological insulator with large spin hall effect for ultralow power spin-orbit torque switching," *Nature materials*, vol. 17, no. 9, pp. 808–813, 2018.
- [23] B. Wu et al., "Field-free 3t2sot mram for non-volatile cache memories," *IEEE Transactions on Circuits and Systems I: Regular Papers*, vol. 67, no. 12, pp. 4660–4669, 2020.
- [24] K. Tsunekawa et al., "Giant tunneling magnetoresistance effect in low-resistance cofeb/mgo(001)/cofeb magnetic tunnel junctions for read-head applications," *Applied Physics Letters*, vol. 87, no. 7, p. 072503, 2005.
- [25] K. Wang, J. Alzate, and P. K. Amiri, "Low-power non-volatile spintronic memory: Stt-ram and beyond," *Journal of Physics D: Applied Physics*, vol. 46, no. 7, p. 074003, 2013.
- [26] Garello, Kevin et al., "Ultrafast magnetization switching by spin-orbit torques," *Applied Physics Letters*, vol. 105, no. 21, 2014.
- [27] Wu, YC et al., "Voltage-gate-assisted spin-orbit-torque magnetic random-access memory for high-density and low-power embedded applications," *Physical Review Applied*, vol. 15, no. 6, p. 064015, 2021.
- [28] Garello, Kevin et al., "Sot-mram 300mm integration for low power and ultrafast embedded memories," in *2018 IEEE Symposium on VLSI Circuits*. IEEE, 2018, pp. 81–82.
- [29] A. Samajdar et al., "A systematic methodology for characterizing scalability of dnn accelerators using scale-sim," in *2020 IEEE International Symposium on Performance Analysis of Systems and Software (ISPASS)*. IEEE, 2020, pp. 58–68.
- [30] A. Parashar et al., "Timeloop: A systematic approach to dnn accelerator evaluation," in *2019 IEEE international symposium on performance analysis of systems and software*. IEEE, 2019, pp. 304–315.
- [31] "Hugging Face." [Online]. Available: <https://huggingface.co/>
- [32] Garello, K. et al., "Manufacturable 300mm platform solution for field-free switching sot-mram," in *2019 Symposium on VLSI Technology*, 2019, pp. T194–T195.
- [33] "Synopsys." [Online]. Available: <https://www.synopsys.com/>
- [34] K. Mishty and M. Sadi, "Designing efficient and high-performance ai accelerators with customized stt-mram," *IEEE Transactions on Very Large Scale Integration Systems*, vol. 29, pp. 1730–1742, 2021.
- [35] M. Poremba et al., "Destiny: A tool for modeling emerging 3d nvm and edram caches," in *Design, Automation Test in Europe*, 2015.
- [36] Y. Seo, K.-W. Kwon, X. Fong, and K. Roy, "High performance and energy-efficient on-chip cache using dual port (1r/1w) spin-orbit torque mram," *IEEE Journal on Emerging and Selected Topics in Circuits and Systems*, vol. 6, no. 3, pp. 293–304, 2016.
- [37] H. Wang et al., "A new mram-based process in-memory accelerator for efficient neural network training with floating point precision," in *IEEE International Symposium on Circuits and Systems*, 2020.
- [38] G. Yuan, X. Ma, S. Lin, Z. Li, and C. Ding, "A sot-mram-based processing-in-memory engine for highly compressed dnn implementation," *arXiv preprint arXiv:1912.05416*, 2019.
- [39] Y. Luo et al., "Performance benchmarking of spin-orbit torque magnetic ram for deep neural network (dnn) accelerators," in *2022 IEEE International Memory Workshop (IMW)*, 2022, pp. 1–4.



**Kaniz Mishty** received the B.S. degree in Electronics and Communication Engineering from Khulna University of Engineering and Technology, Bangladesh, in 2018. She is currently working towards her Ph.D. degree in ECE at Auburn University, AL, USA. Her current research interests are energy and area efficient VLSI system design, AI/Neuromorphic hardware design and AI/ML in CAD. She interned with Apple Inc. in Summer '22 and Qualcomm Tech. in Summer '21. During her internship with Apple she worked on AI application in custom circuit design flow to improve PPA.



**Mehdi Sadi** (S'12-M'17) is an Assistant Professor at the Department of Electrical and Computer Engineering at Auburn University, Auburn, AL. Dr. Sadi earned his PhD in ECE from University of Florida, Gainesville, in 2017, MS from University of California at Riverside, USA in 2011 and BS from Bangladesh University of Engineering and Technology in 2010. Prior to joining Auburn University, he was a Senior R&D SoC Design Engineer at Intel Corporation in Oregon. Dr. Sadi's research focus is on developing algorithms and CAD techniques for implementation, design, reliability, and security of AI hardware. His research also spans into developing Machine Learning/AI enabled design flows for System-on-Chip, and Design-for-Robustness. He has published more than 25 peer-reviewed research papers. He was the recipient of Semiconductor Research Corporation best in session award, Intel Xeon Design Group recognition awards, and National Science Foundation GRII award.